

<sup>1</sup> **neonSoilFlux: An R Package for Continuous  
2 Sensor-Based Estimation of Soil CO<sub>2</sub> Fluxes**

<sup>3</sup> John Zobitz<sup>1</sup>      Edward Ayres<sup>2</sup>      Zoey Werbin<sup>3</sup>      Ridwan Abdi<sup>1</sup>  
<sup>4</sup>                         Natalie Ashburner-Wright<sup>5</sup>      Lillian Brown<sup>5</sup>  
<sup>5</sup> Ryan Frink-Sobierajski<sup>5</sup>      Lajntxiag Lee<sup>1</sup>      Dijonë Mehmeti<sup>1</sup>  
<sup>6</sup>                         Christina Tran<sup>5</sup>      Ly Xiong<sup>1</sup>      Naupaka Zimmerman<sup>4,5</sup>

<sup>7</sup> <sup>1</sup> Augsburg University, 2211 Riverside Avenue, Minneapolis, MN 55454

<sup>8</sup> <sup>2</sup> National Ecological Observatory Network, Battelle, 1685 38th Street, Suite 100, Boulder, CO  
<sup>9</sup> 80301

<sup>10</sup> <sup>3</sup> Boston University, 5 Cummington Street, Boston, MA 02215

<sup>11</sup> <sup>4</sup> University of Kansas, 1450 Jayhawk Boulevard, Lawrence, KS 66045

<sup>12</sup> <sup>5</sup> University of San Francisco, 2130 Fulton Street, San Francisco, CA 94117

<sup>13</sup> **Acknowledgments**

<sup>14</sup> John Zobitz acknowledges Kathleen O'Rourke for code development. Naupaka Zimmerman  
<sup>15</sup> thanks technical staff at USF for support with field gear assembly and shipping. We thank the  
<sup>16</sup> NEON field staff and assignable assets teams for facilitating each of the six NEON site visits.

<sup>17</sup> We are grateful to LI-COR technical staff for helpful discussions about optimal soil chamber  
<sup>18</sup> sampling methods. This work was supported by NSF DEB grant #2017829 awarded to John  
<sup>19</sup> Zobitz, and NSF DEB grant #2017860 awarded to Naupaka Zimmerman. This material is  
<sup>20</sup> based in part upon work supported by the National Ecological Observatory Network (NEON),  
<sup>21</sup> a program sponsored by the U.S. National Science Foundation (NSF) and operated under  
<sup>22</sup> cooperative agreement by Battelle. We also thank the reviewers and subject editor for their  
<sup>23</sup> constructive feedback.

## <sup>24</sup> **Conflict of Interest Statements**

<sup>25</sup> None of the authors have a financial, personal, or professional conflict of interest related to this  
<sup>26</sup> work.

## <sup>27</sup> **Author Contributions**

<sup>28</sup> Conceptualization: John Zobitz, Naupaka Zimmerman; Methodology: Edward Ayres, John  
<sup>29</sup> Zobitz, Naupaka Zimmerman; Software: John Zobitz, Naupaka Zimmerman, Zoey Werbin,  
<sup>30</sup> Edward Ayres, Dijonë Mehmeti, Ridwan Abdi, Ly Xiong, Lajntxiag Lee; Validation: John  
<sup>31</sup> Zobitz, Naupaka Zimmerman; Formal Analysis: John Zobitz, Naupaka Zimmerman, Dijonë  
<sup>32</sup> Mehmeti, Ridwan Abdi, Ly Xiong, Lajntxiag Lee; Investigation: John Zobitz, Naupaka Zimmerman,  
<sup>33</sup> Ryan Frink-Sobierajski, Christina Tran, Natalie Ashburner-Wright, Lillian Brown;  
<sup>34</sup> Resources: John Zobitz, Naupaka Zimmerman; Data curation: John Zobitz, Naupaka Zimmerman,  
<sup>35</sup> Dijonë Mehmeti, Ly Xiong; Writing – original draft: John Zobitz, Naupaka Zimmerman;  
<sup>36</sup> Writing – review and editing: John Zobitz, Naupaka Zimmerman, Zoey Werbin, Edward Ayres,  
<sup>37</sup> Christina Tran, Dijonë Mehmeti, Ly Xiong; Visualization: John Zobitz, Naupaka Zimmerman,

<sup>38</sup> Dijonë Mehmeti, Ridwan Abdi, Ly Xiong; Supervision: John Zobitz, Naupaka Zimmerman;  
<sup>39</sup> Project Administration: John Zobitz, Naupaka Zimmerman; Funding Acquisition: John Zobitz,  
<sup>40</sup> Naupaka Zimmerman.

<sup>41</sup> **Data Availability**

<sup>42</sup> Data available via <https://doi.org/10.5281/zenodo.17516319> (Zobitz & Zimmerman, 2025).  
<sup>43</sup> Field-collected data, `neonSoilFlux` calculated outputs, and manuscript-generating code are  
<sup>44</sup> provided within this repository.

45 **1 Abstract**

- 46 1. Accurate quantification of soil carbon fluxes is essential to reduce uncertainty in estimates  
47 of the terrestrial carbon sink. However, these fluxes vary over time and across ecosystem  
48 types and so it can be difficult to estimate them accurately across large scales. The flux  
49 gradient method estimates soil carbon fluxes using co-located measurements of soil CO<sub>2</sub>  
50 concentration, soil temperature, soil moisture, and other soil properties. The National  
51 Ecological Observatory Network (NEON) provides such data across 20 ecoclimatic domains  
52 spanning the continental U.S., Puerto Rico, Alaska, and Hawai‘i.
- 53 2. We present an R software package (`neonSoilFlux`) that acquires soil environmental data  
54 to compute half-hourly soil carbon fluxes for each soil replicate plot at a given terrestrial  
55 NEON site. To assess the computed fluxes, we visited six focal NEON sites and measured  
56 soil carbon fluxes using a closed-dynamic chamber approach.
- 57 3. Outputs from the `neonSoilFlux` showed agreement with measured fluxes ( $R^2$  between  
58 measured and `neonSoilFlux` outputs ranging from 0.04 to 0.81 depending on calculation  
59 method used); measured outputs generally fell within the range of calculated uncertainties  
60 from the gradient method. Calculated fluxes from `neonSoilFlux` aggregated to the daily  
61 scale exhibited expected site-specific seasonal patterns.
- 62 4. While the flux gradient method is broadly effective, its accuracy is highly sensitive  
63 to site-specific inputs, including the extent to which gap-filling techniques are used to  
64 interpolate missing sensor data and to estimates of soil diffusivity and moisture content.  
65 Future refinement and validation of `neonSoilFlux` outputs can contribute to existing  
66 databases of soil carbon flux measurements, providing near real-time estimates of a critical  
67 component of the terrestrial carbon cycle.

68 **1.1 Keywords**

69 Soil carbon, carbon dioxide, flux gradient, carbon cycle, field validation, soil respiration,  
70 ecosystem variability, diffusion

71 **2 Data for peer review**

72 Anonymous field-collected data, `neonSoilFlux` calculated outputs, and manuscript-generating  
73 code for peer review are provided as supplemental files. An anonymous link for peer-review  
74 is here: <https://doi.org/10.5281/zenodo.16951117>. This will be made publicly available upon  
75 publication.

76 **3 Introduction**

77 Soils contain the planet's largest reservoir of terrestrial carbon (Jobbágy & Jackson, 2000). A  
78 critical component of this reservoir is soil organic matter, the accumulation of which is influenced  
79 by biotic factors such as above-ground plant inputs (Jackson et al., 2017). These inputs in  
80 turn are influenced by environmental factors such as growing season length, temperature, and  
81 moisture (Desai et al., 2022), which also affect the breakdown of soil organic matter and its  
82 return to the atmosphere. Across heterogeneous terrestrial landscapes, the interplay between  
83 these biotic and abiotic factors influence the size of the soil contribution to the terrestrial  
84 carbon sink (Friedlingstein et al., 2025). However, the heterogeneity of these processes across  
85 diverse ecosystems in the context of rapid environmental change leads to large uncertainty  
86 about the magnitude of this sink in the future, and thus there remains a pressing need to  
87 quantify changes in soil carbon pools and fluxes across scales.

88 Ecological observation networks such as the United States' National Ecological Observatory  
89 Network (NEON) and others (e.g. the globally-distributed FLUXNET or the European Inte-  
90 grated Carbon Observation System) present a significant advancement in the nearly continuous  
91 observation of biogeochemical processes at the continental scale. Notably, at 47 terrestrial  
92 sites across the continental United States that span 20 ecoclimatic domains, NEON provides  
93 half-hourly measurements of soil CO<sub>2</sub> concentration, temperature, and moisture at different  
94 vertical depths. Each of these NEON sites also encompasses measurements of the cumulative  
95 sum of all ecosystem carbon fluxes in an airshed using the eddy covariance technique (Baldocchi,  
96 2014). Soil observations provided by NEON are on the same timescale and standardized with  
97 eddy covariance measurements from FLUXNET. These types of nearly continuous observational  
98 data (NEON and FLUXNET) can be used to reconcile differences between model-derived  
99 or data-estimated components of ecosystem carbon flux (Jian et al., 2022; Luo et al., 2011;  
100 Phillips et al., 2017; J. Shao et al., 2015; P. Shao et al., 2013; Sihi et al., 2016).

101 Estimated or observed soil carbon fluxes are a key metric for understanding change in soil  
102 carbon pools over time (Bond-Lamberty et al., 2024). A soil carbon flux to the atmosphere ( $F_S$ ,  
103 units  $\mu\text{mol m}^{-2} \text{s}^{-1}$ ), represents the aggregate process of transfer of soil CO<sub>2</sub> to the atmosphere  
104 from physical and biological processes (e.g. diffusion and respiration). Soil carbon fluxes can  
105 be assumed to encompass soil carbon respiration from autotrophic or heterotrophic sources  
106 (Davidson et al., 2006) and modeled with a exponential  $Q_{10}$  paradigm (Bond-Lamberty et al.,  
107 2004; Chen & Tian, 2005; Hamdi et al., 2013).

108 One common method by which  $F_S$  is measured in the field is through the use of soil chambers  
109 in a closed, well-mixed system (Norman et al., 1997) with headspace trace gas concentrations  
110 measured with an infrared gas analyzer (IRGA).  $F_S$  can also be estimated from soil CO<sub>2</sub>  
111 measurements at different depths in the soil using the flux-gradient method (Maier & Schack-  
112 Kirchner, 2014). Closed-chamber IRGA measurements, while being the most common method,

113 require either frequent in-person site visits or expensive and fragile automated systems. The  
114 potential of the gradient method is that fluxes can be estimated from continuous data recorded  
115 by robust solid-state sensors. The flux-gradient method is an approach that uses conservation of  
116 mass to calculate flux at a vertical soil depth  $z$  at steady state by applying Fick's law of diffusion.  
117 A simplifying assumption for the flux-gradient method is that there is no mass transfer in the  
118 other spatial dimensions  $x$  and  $y$  (Maier & Schack-Kirchner, 2014). The diffusivity profile, a  
119 key component of this calculation, varies across the soil depth as a function of soil temperature,  
120 soil volumetric water content, atmospheric air pressure, and soil bulk density (Millington &  
121 Shearer, 1971; Moldrup et al., 1999; Sallam et al., 1984).

122 Databases such as the Soil Respiration Database (SRDB) or the Continuous Soil Respiration  
123 Database (COSORE) add to the growing network of resources for making collected observations  
124 of soil fluxes available to other researchers (Bond-Lamberty, 2018; Bond-Lamberty et al., 2020;  
125 Bond-Lamberty & Thomson, 2010; Jian et al., 2021; Jiang et al., 2024). However, these  
126 databases currently encompass primarily direct soil measurements of fluxes (i.e. those using  
127 methods like the closed-chamber method described above). Currently, NEON provides all  
128 measurements to calculate  $F_S$  from Fick's law, but soil flux as a derived data product was  
129 descoped from the initial network launch due to budget constraints (Berenbaum et al., 2015).  
130 Deriving estimates of  $F_S$  using continuous sensor data across NEON sites using NEON data  
131 thus remains a high priority.

132 This study describes an R software package, `neonSoilFlux`, that computes a standardized  
133 estimate of  $F_S$  at all terrestrial NEON sites using the flux-gradient method. Using direct  
134 chamber-based field observations of soil carbon dioxide flux from a subset of terrestrial NEON  
135 sites spanning six states, we provide a direct validation of  $F_S$  from `neonSoilFlux`. While  
136 open source R software tools currently exist for processing chamber-based flux measurements  
137 (Jurasinski et al., 2022; Pedersen, 2024; Rheault et al., 2024; Wilson et al., 2024; Zhao, 2019),

138 to our knowledge this is the first package that incorporates NEON data directly.

139 Key objectives of this study are to:

- 140 1. Apply the flux-gradient method to estimate soil CO<sub>2</sub> flux from continuous sensor mea-
- 141 surements across six NEON sites.
- 142 2. Benchmark estimated soil carbon fluxes against field measurements (e.g. direct chamber
- 143 measurements of soil flux).
- 144 3. Identify sources of error in the flux-gradient approach across diverse sites in order to
- 145 guide future work.

## 146 **4 Materials and Methods**

### 147 **4.1 Field methods**

#### 148 **4.1.1 Focal NEON Sites**

149 In order to acquire field data to validate model predictions of flux, we selected six terrestrial  
150 NEON sites for analysis. We conducted roughly week-long field measurement campaigns at  
151 these sites, which span a range of environmental gradients and terrestrial domains (Table 1).  
152 SJER, SRER, and WREF were visited during May and June of 2022, and WOOD, KONZ,  
153 and UNDE during May and June of 2024.

#### 154 **4.1.2 Soil collar placement**

155 Either one (2022 sampling campaign) or two (2024 sampling campaign) PVC soil collars (20.1  
156 cm inside diameter) were installed in close proximity to the permanent NEON soil sensors at

157 each site (Figure 1). As instruments in the NEON soil sensor arrays can occasionally break  
158 down or stop working, the specific soil plot where we made measurements was chosen at each  
159 site in consultation with NEON staff to maximize likelihood of quality soil sensor measurements  
160 during the duration of the IRGA measurements. The plot selected at each site (out of the 5 in  
161 each replicate array at each site) are presented in the last column of Table 1. After installation,  
162 collar(s) were left to equilibrate for approximately 24 hours prior to any measurements being  
163 taken.

164 **4.1.3 Infrared gas analyzer measurements of soil CO<sub>2</sub> flux**

165 In 2022, we then made measurements of flux on an hourly interval for 8 hours each day.  
166 Measurements were taken from roughly 8 am to 4 pm, with the time interval selected to  
167 capture the majority of the diurnal gradient of soil temperature each day. These measurements  
168 were made using a LI-6800 infrared gas analyzer instrument (LI-COR Environmental, Lincoln,  
169 NE) fitted with a soil chamber attachment (attachment 6800-09). In 2024, we again used the  
170 same LI-6800 instrument, but made half-hourly measurements over an approximately 8 hour  
171 period. In addition, in 2024 we also installed a second collar and used a second instrument, an  
172 LI-870 CO<sub>2</sub> IRGA, connected to an automated robotic chamber (LI-COR chamber 8200-104)  
173 controlled by an LI-8250 multiplexer to make automated measurements. The multiplexer was  
174 configured to take half-hourly measurements 24 hours a day for the duration of our sampling  
175 bout at each site. Each instrument was paired with a soil temperature and moisture probe  
176 (Stevens HydraProbe, Stevens Water, Portland, OR) that was used to make soil temperature  
177 and moisture measurements concurrent with the CO<sub>2</sub> flux measurements. Chamber volumes  
178 were set by measuring collar offsets at each site. System checks were conducted daily for the  
179 LI-6800 and weekly for the LI-8250. Instruments were factory calibrated before each field  
180 season.

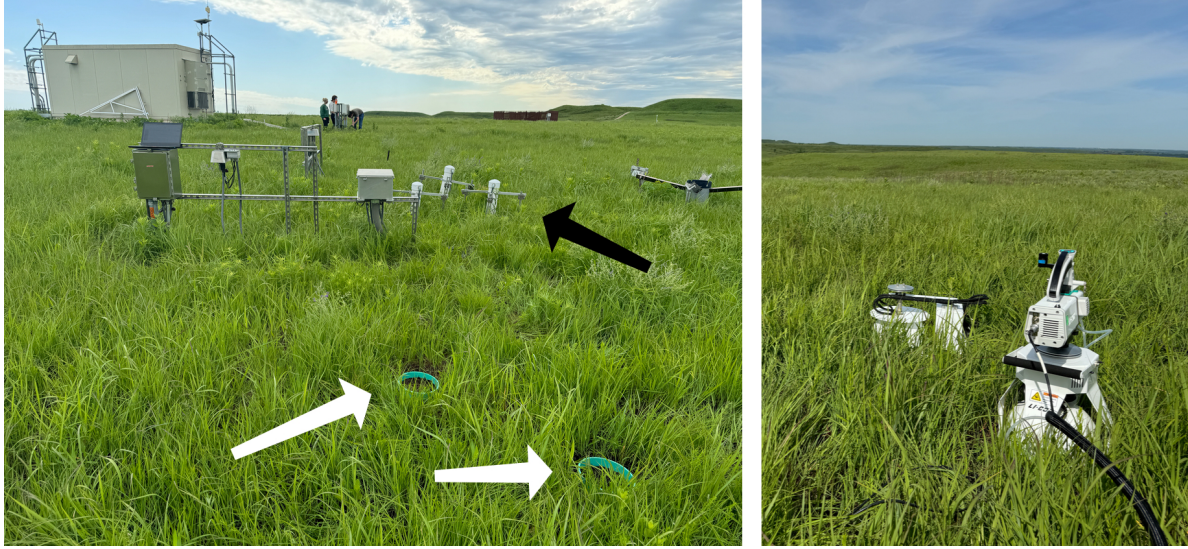


Figure 1: Spatial layout of field sampling using a closed-dynamic chamber setup at a representative NEON site (KONZ). Left image shows collars (white arrows) and permanent soil sensor installation (black arrow) and right image shows the LI-6800 (foreground) and LI-8200-104 (background) instruments placed on the collars.

Table 1: Listing of NEON sites studied for field work and analysis. Site refers to NEON site codes: Santa Rita Experimental Range (SRER), San Joaquin Experimental Range (SJER), Wind River Experimental Forest (WREF), Chase Lake National Wildlife Refuge (WOOD), Konza Prairie Biological Station (KONZ), and the University of Notre Dame Environmental Research Center (UNDE). Location is reported in decimal degrees of latitude and longitude. Other abbreviations include Mean Annual Temperature (MAT);  $\overline{T_S}$ : average soil temperature during field measurements;  $\overline{SWC}$ : average soil water content during field measurements. Dates refer to field measurement dates for each site. Plot refers to the particular location in the soil sensor array (denoted as HOR by NEON) where field measurements were made.

Site	Location	Ecosystem	MAT	$\overline{T_S}$	MAP	$\overline{SWC}$	Dates	Plot
SRER	31.91068, -110.83549	Shrubland	19.3 °C	47.6 °C	346 mm	4.0%	May 29– June 1 2022	004
SJER	37.10878, -119.73228	Oak woodland	16.4 °C	41.7 °C	540 mm	1.2%	June 1–4 2022	005
WREF	45.82049, -121.95191	Evergreen forest	9.2 °C	15.3 °C	2225 mm	27.2%	June 7–9 2022	001
WOOD	47.1282, -99.241334	Restored prairie	4.9 °C	14.9 °C	495 mm	14.9%	June 3–9 2024	001
KONZ	39.100774, -96.563075	Tallgrass prairie	12.4 °C	23.4 °C	870 mm	23.4%	May 29– June 1 2024	001

Table 1: Listing of NEON sites studied for field work and analysis. Site refers to NEON site codes: Santa Rita Experimental Range (SRER), San Joaquin Experimental Range (SJER), Wind River Experimental Forest (WREF), Chase Lake National Wildlife Refuge (WOOD), Konza Prairie Biological Station (KONZ), and the University of Notre Dame Environmental Research Center (UNDE). Location is reported in decimal degrees of latitude and longitude. Other abbreviations include Mean Annual Temperature (MAT);  $\bar{T}_S$ : average soil temperature during field measurements;  $\bar{SWC}$ : average soil water content during field measurements. Dates refer to field measurement dates for each site. Plot refers to the particular location in the soil sensor array (denoted as HOR by NEON) where field measurements were made.

Site	Location	Ecosystem	MAT	$\bar{T}_S$	MAP	$\bar{SWC}$	Dates	Plot
UNDE	46.23391, -89.537254	Deciduous forest	4.3 °C	13.0 °C	802 mm	13.0%	May 22–25 2024	004

#### 181 4.1.4 Post-collection processing of field data

182 We used LI-COR SoilFluxPro software (v 5.3.1) to assess the data after collection and to  
 183 inform sampling parameters. We checked appropriateness of dead band and measurement  
 184 durations using built-in evaluation tools. Based on this, the deadband period was set for 30-40  
 185 seconds, depending on the site, and the measurement duration was 180 seconds with a 30  
 186 second pre-purge and a 30 second post-purge at most sites, and a 90 second pre- and post-purge  
 187 at sites with higher humidity due to recent precipitation events. We also assessed the  $R^2$  of  
 188 linear and exponential model fits to measured CO<sub>2</sub> to verify measurement quality.

#### 189 4.2 neonSoilFlux R package

190 We developed an R package called `neonSoilFlux` (Zobitz et al., 2024) to compute half-hourly  
 191 soil carbon fluxes and uncertainties from NEON data. The objective of the `neonSoilFlux`  
 192 package is a unified workflow (Figure 2) for soil data acquisition and analysis that supplements  
 193 the existing `neonUtilities` data acquisition R package (Lunch et al., 2025).

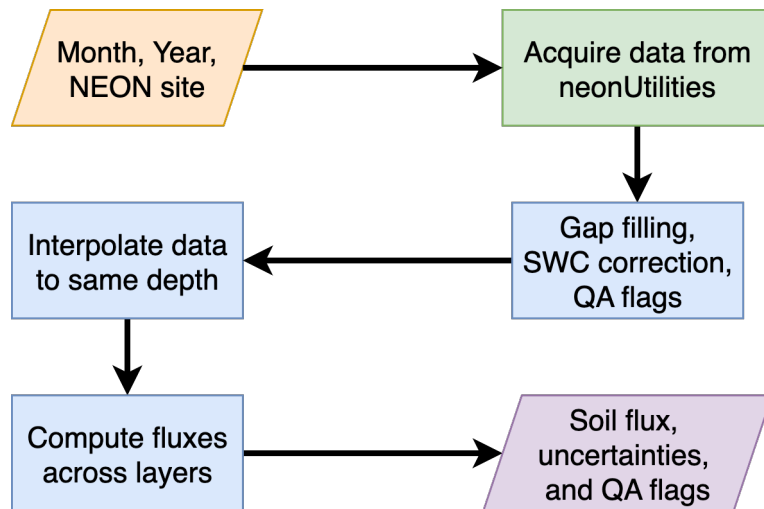


Figure 2: Diagram of `neonSoilFlux` R package. For a given month, year, and NEON site (orange parallelogram), the package acquires all relevant data to compute  $F_S$  using the `neonUtilities` R package (green rectangle). Data are gap-filled according to reported QA flags and adjusted for changes in soil water content (SWC) calibration coefficients, then interpolated to the same measurement depth before computing the soil flux, uncertainties, and final QA flags (blue rectangles). The package reports the associated soil flux, uncertainties, and quality assurance (QA) flags for the user (purple parallelogram).

194 At a given NEON site there are five replicate soil plots, each with measurements of soil  
 195  $\text{CO}_2$  concentration, soil temperature, and soil moisture at different depths (Figure 3). The  
 196 `neonSoilFlux` package acquires measured soil  $\text{CO}_2$  concentration (NEON, 2024b), soil temper-  
 197 ature (NEON, 2024d), soil water content (NEON, 2024e), barometric pressure from the nearby  
 198 tower (NEON, 2024a), and soil properties (e.g. bulk density) (NEON, 2024c) from a range of  
 199 different NEON data products. The static soil properties were collected by NEON staff from a  
 200 nearby soil pit during initial site characterization and are assumed to be constant at each site.  
 201 A soil flux calculation is computed at each replicate soil plot.

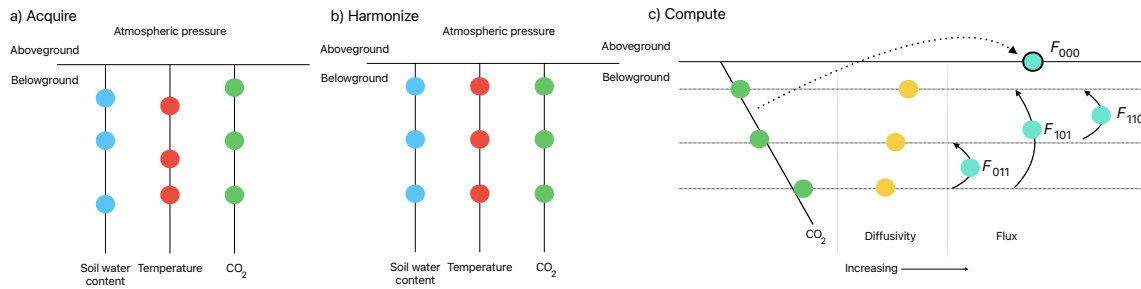


Figure 3: Model diagram of the data workflow for the `neonSoilFlux` R package. a) Acquire: Data are obtained for a given NEON location and horizontal sensor location, which includes soil water content, soil temperature,  $\text{CO}_2$  concentration, and atmospheric pressure. All data are screened for quality assurance; if gap-filling of missing data occurs, it is flagged for the user. b) Harmonize: Any belowground data are then harmonized to the same depth as  $\text{CO}_2$  concentrations using linear regression. c) Compute: The flux across a given depth is computed via Fick's law, denoted with  $F_{ijk}$ , where  $i$ ,  $j$ , or  $k$  are either 0 or 1 denoting the layers the flux is computed across ( $i$  = closest to surface,  $k$  = deepest).  $F_{000}$  represents a flux estimate where the gradient  $dC/dz$  is the slope of a linear regression of  $\text{CO}_2$  with depth.

202 The workflow to compute a value of  $F_S$  with `neonSoilFlux` consists of three primary steps,  
 203 illustrated in Figure 3. First, NEON data are acquired for a given site and month via the  
 204 `neonUtilities` R package (yellow parallelogram and green rectangle in Figure 2 and Panel a  
 205 in Figure 3). Acquired environmental data can be exported to a comma separated value file for  
 206 additional analysis. Quality assurance (QA) flags are reported as an indicator variable. Since

207 the calibration coefficients on the soil water content sensors have changed over time (NEON,  
208 2024e), raw sensor measurements were back-calculated and soil-specific calibrations were applied  
209 following Ayres et al. (2024) to generate a consistent time series at each measurement location.

210 The second step is harmonizing the data to compute soil fluxes across soil layers. This  
211 step consists of three different actions (blue rectangles in Figure 2 and Panel b in Figure 3).  
212 If a given observation by NEON is reported as not passing a quality assurance check, we  
213 applied a gap filling method to replace that measurement with its monthly mean at that same  
214 depth (Section 4.2.1). Belowground measurements of soil water and soil temperature are then  
215 interpolated to the same depth as soil CO<sub>2</sub> measurements. The diffusivity (Section 4.2.2) and  
216 soil flux across different soil layers (Section 4.2.3) are then computed.

217 The third and final step is computing a surface soil flux through extrapolation to the surface  
218 (purple parallelogram in Figure 2 and Panel c in Figure 3). Uncertainty on a soil flux  
219 measurement is computed through quadrature. An aggregate quality assurance (QA) flag for  
220 each environmental measurement is also reported, representing if any gap-filled measurements  
221 were used in the computation of a soil flux. Within the soil flux-gradient method, several  
222 different approaches can be used to derive a surface flux (Maier & Schack-Kirchner, 2014); the  
223 `neonSoilFlux` package reports four different possible values for soil surface flux (Section 4.2.3)  
224 for each of two different methods of diffusivity estimation, for a total of eight estimates of  
225 flux.

#### 226 4.2.1 Gap-filling routine

227 NEON reports QA flags as binary values for each measurement and half-hourly interval. For a  
228 given half-hour, if any input variable (soil CO<sub>2</sub> concentration, soil temperature, or soil moisture)  
229 at depth  $z$  is flagged, computation of  $F_S$  is not possible. To address this, flagged measurements

230 and their uncertainties were replaced with a bootstrapped monthly mean ( $\bar{m}$ ) and monthly  
231 standard deviation ( $\bar{s}$ ) (Efron & Tibshirani, 1994).

232 For each month, depth  $z$ , and variable, we computed bootstrapped estimates of  $\bar{m}$  and  $\bar{s}$   
233 from the vectors of unflagged measurements ( $\mathbf{m}$ ), reported standard errors ( $\sigma$ ), and the 95%  
234 confidence interval ( $\epsilon$ , or expanded uncertainty; Farrance & Frenkel (2012)). We also defined a  
235 bias vector  $\mathbf{b} = \sqrt{\epsilon^2 - \sigma^2}$ , which quantifies the spread of uncertainty in a given period and is  
236 incorporated into  $\bar{m}$ .

237 From these, 5000 bootstrap samples were generated for  $\mathbf{m}$ ,  $\sigma$ , and  $\mathbf{b}$ . For each sample ( $m_k, b_k, \sigma_k$ ),  
238 we generated a vector  $\mathbf{n}$  (length  $N = 5000$ ) by drawing from a normal distribution with mean  
239  $m_k + b_k$  and standard deviation  $\sigma_k$ . The sample mean and standard deviation were then  
240 computed from  $\mathbf{n}$ . The resulting distributions of sample means and sample standard deviations  
241 provided the bootstrapped monthly mean ( $\bar{m}$ ) and standard error ( $\bar{s}$ ) respectively.

242 This gap-filling procedure provides a consistent treatment across all data streams. However,  
243 alternative approaches may be better suited for longer gaps (e.g., correlations with other NEON  
244 measurement levels or soil plots) or for variable-specific conditions. We discuss the effect of  
245 gap-filling on our results in Section 6.1.

246 **4.2.2 Soil diffusivity**

247 Soil diffusivity  $D_a$  at a given measurement depth is the product of the diffusivity in free air  
248  $D_{a,0}$  ( $\text{m}^2 \text{ s}^{-1}$ ) and the tortuosity  $\xi$  (no units) (Millington & Shearer, 1971).

249 We compute  $D_{a,0}$  with Equation 1:

$$D_{a,0} = 0.0000147 \cdot \left( \frac{T_i + 273.15}{293.15} \right)^{1.75} \cdot \left( \frac{P}{101.3} \right) \quad (1)$$

250 where  $T_i$  is soil temperature ( $^{\circ}\text{C}$ ) at depth  $i$  (NEON, 2024d) and  $P$  surface barometric pressure  
251 (kPa) (NEON, 2024a).

252 Previous studies by Sallam et al. (1984) and Tang et al. (2003) demonstrated the sensitivity  
253 of modeled  $F_S$  depending on the tortuosity model ( $\xi$ ) used to compute diffusivity. At low  
254 soil water content, the choice of tortuosity model can lead to order-of-magnitude differences  
255 in  $D_a$ , which in turn affect modeled  $F_S$ . The `neonSoilFlux` package currently includes two  
256 approaches to calculate  $\xi$ , representing the range of tortuosity behavior reported in Sallam et  
257 al. (1984).

258 The first approach is the Millington-Quirk model (Millington & Shearer, 1971), in which  
259 tortuosity depends on both porosity and soil water content:

$$\xi = \frac{(\phi - SWC_i)^{10/3}}{\phi^2} \quad (2)$$

260 In Equation 2,  $SWC$  is the soil water content at depth  $i$  (NEON, 2024e) and  $\phi$  is the porosity,  
261 which in turn is a function of soil physical properties (NEON, 2024c):

$$\phi = \left(1 - \frac{\rho_s}{\rho_m}\right) (1 - f_V) \quad (3)$$

262 In Equation 3,  $\rho_m$  is the particle density of mineral soil ( $2.65 \text{ g cm}^{-3}$ ),  $\rho_s$  the soil bulk density  
263 ( $\text{g cm}^{-3}$ ) excluding coarse fragments greater than 2 mm (NEON, 2024c), and  $f_V$  is a site-specific  
264 value that accounts for the proportion of soil fragments between 2-20 mm. Soil fragments  
265 greater than 20 mm were not estimated due to limitations in the amount of soil that can be  
266 analyzed (NEON, 2024c). We assume that rock fragments contain no internal pores.

267 The Millington-Quirk model assumes  $\xi$  is modulated by the amount of fluid saturation in soil  
268 pores (Millington & Shearer, 1971). In contrast, the Marshall model (Marshall, 1959) expresses  
269 tortuosity as only a function of porosity ( $\xi = \phi^{1.5}$ ), with  $\phi$  defined from Equation 3. The  
270 Marshall model is independent of soil water content and assumes tortuosity is only governed  
271 by soil structure. The `neonSoilFlux` package allows users to choose the tortuosity model most  
272 appropriate for site-specific conditions and research goals.

273 **4.2.3 Soil flux computation**

274 We applied Fick's law (Equation 4) to compute the soil flux  $F_{ij}$  ( $\mu\text{mol m}^{-2} \text{s}^{-1}$ ) across two soil  
275 depths  $i$  and  $j$ :

$$F_{ij} = -D_a \frac{dC}{dz} \quad (4)$$

276 where  $D_a$  is the diffusivity ( $\text{m}^2 \text{s}^{-1}$ ) and  $\frac{dC}{dz}$  is the gradient of  $\text{CO}_2$  molar concentration ( $\mu\text{mol}$   
277  $\text{m}^{-3}$ , so the gradient has units of  $\mu\text{mol m}^{-3} \text{m}^{-1}$ ). The soil surface flux is theoretically defined  
278 by applying Equation 4 to measurements collected at the soil surface and directly below the  
279 surface. Measurements of soil temperature, soil water content, and soil  $\text{CO}_2$  molar concentration  
280 across the soil profile allow for application of Equation 4 across different soil depths. Each  
281 site had three measurement layers, so we denote the flux as a three-digit subscript  $F_{ijk}$  with  
282 indicator variables  $i$ ,  $j$ , and  $k$  indicate if a given layer was used (written in order of increasing  
283 depth), according to the following:

- 284 •  $F_{000}$  is a surface flux estimate using the intercept of the linear regression of  $D_a$  with  
285 depth and the slope from the linear regression of  $\text{CO}_2$  with depth (which represents  $\frac{dC}{dz}$

286 in Fick's Law). Tang et al. (2003) used this approach to compute fluxes in an oak-grass  
287 savannah.

- 288 •  $F_{110}$  is a flux estimate across the two shallowest measurement layers.
- 289 •  $F_{011}$  is a flux estimate across the two deepest measurement layers.
- 290 •  $F_{101}$  is a flux estimate across the shallowest and deepest measurement layers.

291 For  $F_{110}$ ,  $F_{011}$ , and  $F_{101}$ , the diffusivity used in Fick's Law is always at the deeper measurement  
292 layer. When used as a surface flux estimate we assume CO<sub>2</sub> remains constant above this flux  
293 depth. Uncertainty in all  $F_{ijk}$  values was quantified using quadrature (Taylor, 2022). These  
294 computed fluxes could provide the basis for additional soil flux estimates. For example, Tang et  
295 al. (2005) estimated surface flux by linearly extrapolating  $F_{110}$  and  $F_{011}$  to the soil surface.

### 296 4.3 Post processing evaluation

297 Following collection of field measurements and calculation of the soil fluxes from `neonSoilFlux`  
298 package, we compared measured  $F_S$  based on closed-dynamic chamber measurements with the  
299 LI-COR instruments to a given soil flux calculation from `neonSoilFlux` for each site and flux  
300 computation method and quantified the relationship statistically ( $R^2$ ). Finally, for a half-hourly  
301 interval we also computed a *post hoc* diffusivity ( $D_a$ ) using the LI-COR flux along with the  
302 CO<sub>2</sub> surface gradient reported by NEON using the measurement levels closest to the surface.

Table 2: Summary of measured soil characteristics and flux results from field measurements across six NEON sites using a LI-COR 6800 (LI-870/8250 measurements omitted to enable direct comparability) via the closed-dynamic chamber method. Numeric values for soil CO<sub>2</sub> flux, soil temperature, and volumetric soil water content (VSWC) are the mean and standard deviation of field measurements at each site.

Site	Flux μmol m <sup>-2</sup> s <sup>-1</sup>	Soil temp °C	VSWC cm <sup>3</sup> cm <sup>-3</sup>	n
UNDE	2.55 ± 0.26	14.33 ± 0.77	0.33 ± 0.02	61
WOOD	3.02 ± 0.4	16.01 ± 1.54	0.28 ± 0.01	53
WREF	3.62 ± 0.3	15.34 ± 1.76	0.27 ± 0.06	21
KONZ	6.35 ± 0.97	27.28 ± 4.14	0.37 ± 0.01	44
SJER	0.94 ± 0.02	41.68 ± 11.22	0.01 ± 0.01	32
SRER	0.72 ± 0.09	47.64 ± 7.46	0.04 ± 0.01	32

## 5 Results

### Concordance between modelled and measured soil CO<sub>2</sub> flux

The sites we visited ranged substantially in both their annual average temperature and precipitation as well as their biome type (Table 2). These differences also influenced the wide range of observed flux rates across sites.

The timeseries of the measured fluxes from the LI-COR 6800 and 870/8250 were compared to modeled soil fluxes from the `neonSoilFlux` R package (Figure 4). We also assessed year-long estimated flux time series and compared those to field measurements made at each site (Figure 5). Results are reported in local time. Where applicable, sites are displayed from left to right by increasing soil temperature (Table 1). Positive values of the flux indicate that there is a flux moving towards the surface. Overall, with the exception of SRER (discussed later) the computed fluxes determined using a variety of plausible methods spanned the field-measured fluxes, but the specific flux-gradient method that best approximated field measurements varied by site.

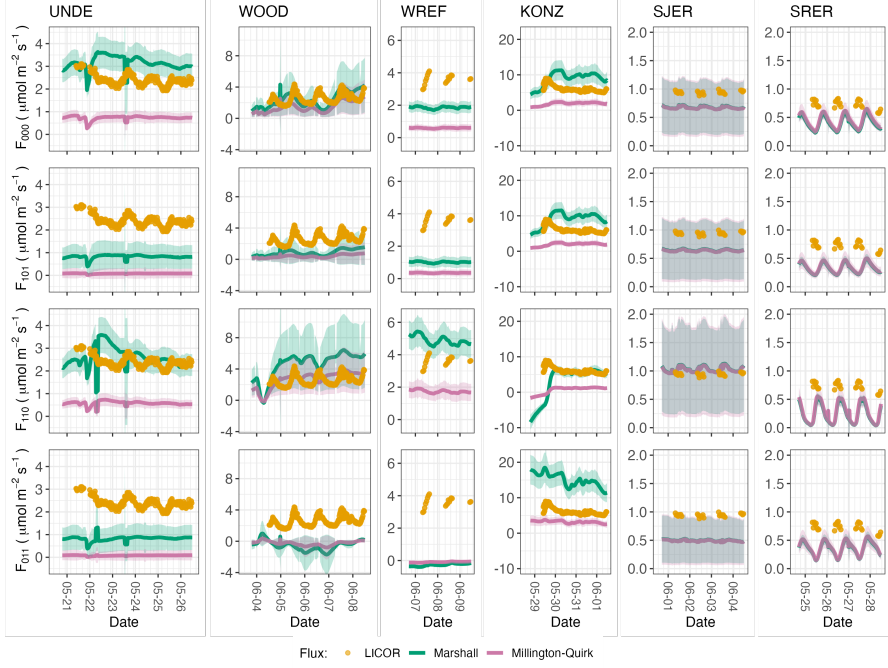


Figure 4: Timeseries of soil surface flux ( $F_S$ ) from field-measured (yellow lines) and modeled soil fluxes (green or purple lines) by the `neonSoilFlux` R package. Fluxes from the `neonSoilFlux` R package are separated by the diffusivity model used (Millington-Quirk or Marshall, Section 4.2.2). Individual vertical axis labels in the first column represent the measurement levels where the flux-gradient approach is applied (Section 4.2.3). Ribbons for modeled soil fluxes represent  $\pm 1$  standard deviation. Results are reported in local time. WREF, SJER, and SRER were sampled in 2022, and UNDE, WOOD, and KONZ were sampled in 2024. Sites (columns) are arranged from left to right in terms of increasing mean annual temperature.

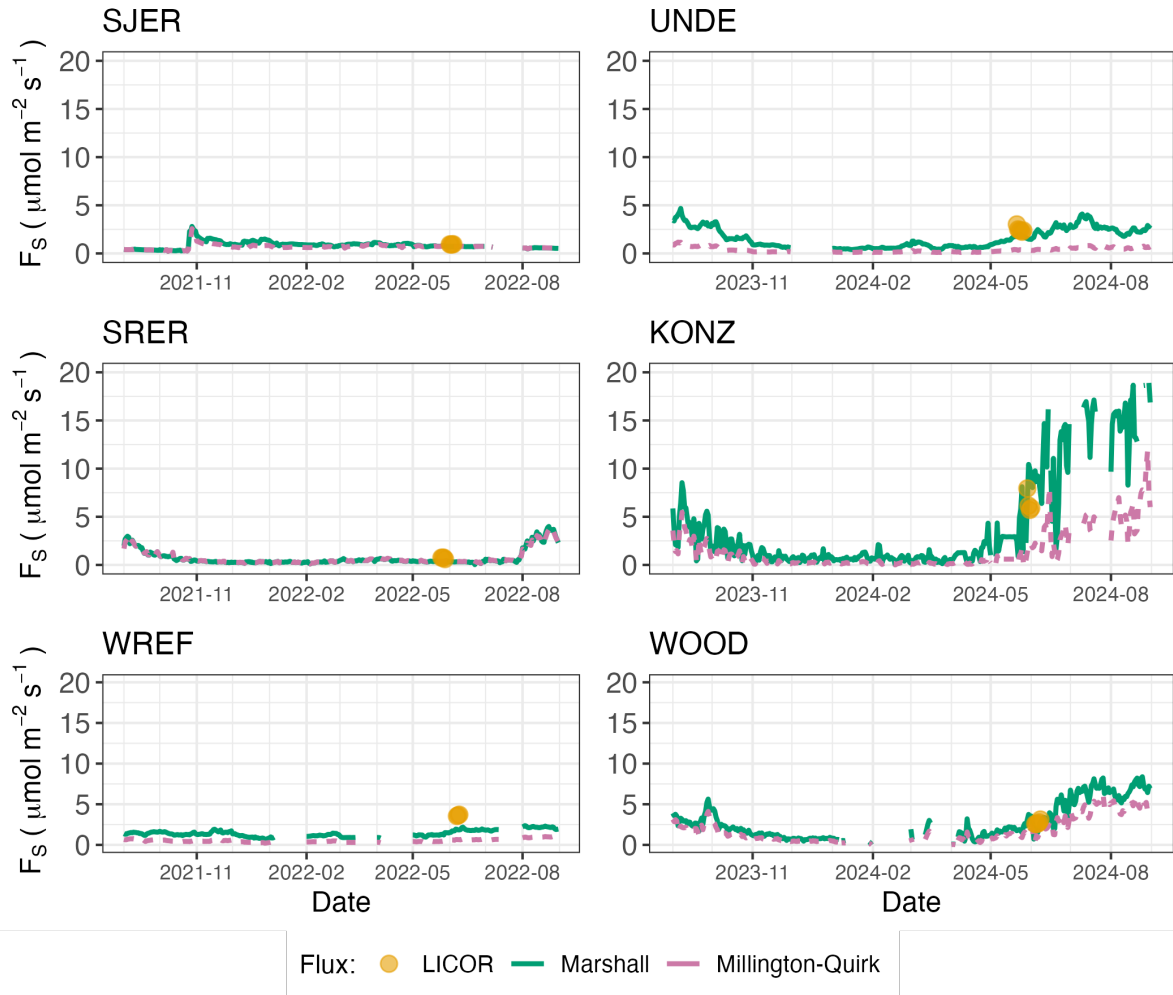


Figure 5: Timeseries of both daily-averaged field  $F_S$  (yellow circles) and daily ensemble averaged soil fluxes (average of  $F_{000}$ ,  $F_{101}$ ,  $F_{011}$ ,  $F_{110}$ , Section 4.2.3) by the `neonSoilFlux` R package, separated by the diffusivity model used (green or purple lines, Millington-Quirk or Marshall, Section 4.2.2).

317 We calculated a statistical relationship between the various estimates of soil flux computed by  
318 `neonSoilFlux` and the field-measured fluxes within daily interval periods. Statistics for these  
319 comparisons are reported in Figure 6, which also shows how these fall relative to a 1:1 line.

320 **5.2 Effects of method choice on diffusivity estimates**

321 In four of six field sites, the *post hoc*  $D_a$  estimate fell roughly between the two diffusion  
322 estimation methods; however this was less the case in the two driest sites, SJER and SRER  
323 (Table 1), where the field estimate of diffusivity was either lower or higher than both of the  
324 other methods (Figure 7).

325 **6 Discussion**

326 This study presents a unified data science workflow to efficiently process automated measure-  
327 ments of belowground soil CO<sub>2</sub> concentrations, soil water content, and soil temperature to  
328 infer estimates of soil surface CO<sub>2</sub> effluxes through application of Fick's Law (Equation 4).  
329 Our core goals in this study were: (1) to generate estimates of soil flux from continuous soil  
330 sensor data at terrestrial NEON sites using the flux-gradient method and then (2) to compare  
331 those estimates to field-measured fluxes based on the closed chamber approach at six NEON  
332 focal sites. We discuss our progress toward these core goals through (1) an overall evaluation  
333 of the flux-gradient approach (and uncertainty calculation) and (2) site-specific evaluation of  
334 differences in estimated vs measured fluxes.

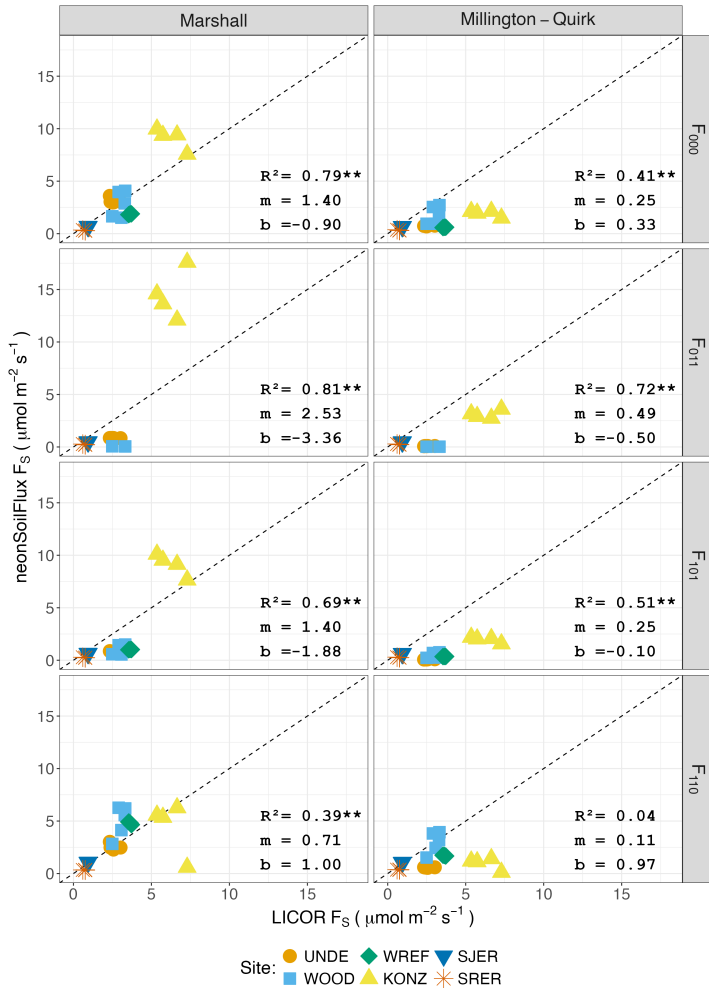


Figure 6: Statistical comparison between measured fluxes at each NEON site with fluxes reported by `neonSoilFlux` with the different flux calculation approaches and diffusivity calculations applied. Points are daily averages and LICOR  $F_S$  values are from the 6800 instrument only, for consistency. The dotted line represents a 1:1 relationship, and the reported  $R^2$  quantifies the relationship between field-measured and `neonSoilFlux` estimated fluxes. \* = significance at the 5% level, \*\* = significance at the 1% level. The slope ( $m$ ) and intercept ( $b$ ) of the linear regression between measured and modeled fluxes are also reported. The low-value outlier from KONZ in the  $F_{110}$  Marshall plot is an example of the effect of inverted CO<sub>2</sub> gradients causing an estimated flux to be negative, bringing down the daily mean, which later resolved as the soils dried back out. Intervals where calculated fluxes were < 0 ( $n = 12$ ) were excluded from the plot; 3 each from WREF and WOOD when using ( $F_{011}$  approach).

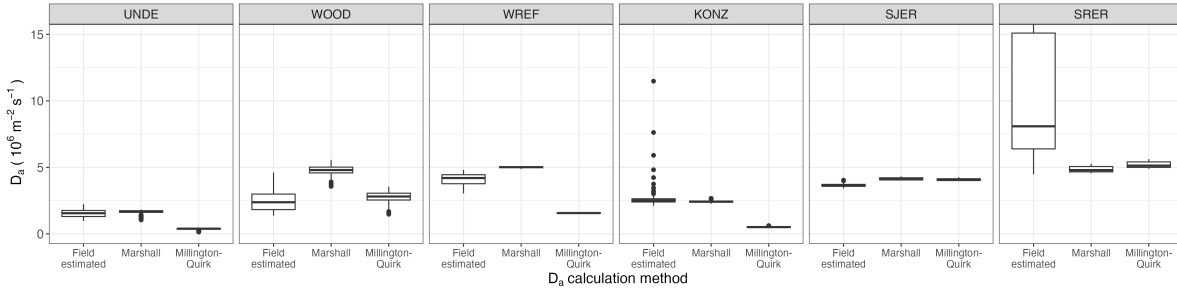


Figure 7: Distribution of diffusivity ( $D_a$ ) at each study site. Values of  $D_a$  were provided by the `neonSoilFlux` package, computed from the Millington-Quirk or Marshall models (Section 4.2.2). A post-hoc estimate of diffusivity (labeled as “Field estimated”) was computed through the field measured flux (Figure 4), divided by the CO<sub>2</sub> gradient from the measurement levels closest to the soil surface, as reported by NEON. We only used  $F_S$  measured by the LICOR 6800 at all sites to standardize comparisons. Some outliers ( $n = 2$  from the field estimated values at KONZ and  $n = 9$  from field estimated values at SRER) are excluded from the plot to allow better comparative visualization across sites.

### 335 6.1 General evaluation of flux-gradient approach

336 Key assumptions of the flux-gradient approach are that CO<sub>2</sub> concentrations increase throughout  
 337 the soil profile such that the highest concentrations are observed in the deepest layers. Addition-  
 338 ally, field flux measurements should correlate with  $F_{000}$  because they represent surface fluxes.

339 Periods where this gradient condition are not met generally are connected to processes that occur  
 340 during soil wetting events, where more shallow soil layers produce higher concentrations of CO<sub>2</sub>  
 341 due to microbial respiration pulses following rewetting. This effect is likely to be largest at sites  
 342 with rich organic soils (e.g. KONZ). Based on this reasoning, in these types of situations we would  
 343 *a priori* expect  $F_{011}$  (deepest layers)  $\leq F_{101} \leq F_{110}$  (shallow layers)  $\leq F_{000}$  (all layers) be-  
 344 cause the previous flux estimates rely primarily on CO<sub>2</sub> concentrations at deeper depths, and  
 345 could miss high concentrations of CO<sub>2</sub> produced in shallower layers.

346 When modeling soil respiration, typically a non-linear response function that also considers soil  
 347 type is used (Bouma & Bryla, 2000; Yan et al., 2016, 2018). For the `neonSoilFlux` package,

348 soil type is connected to the measurement of bulk density, which was characterized at each  
349 NEON site. This bulk density estimate is based on replicate samples collected from the site  
350 megapit at a subset of soil horizons, with an estimated uncertainty of  $\pm 5\%$  (NEON, 2024c).  
351 Coarse fragment estimates also have very large uncertainties, but because the volume fraction  
352 tends to be low in surface soils it is unlikely to contribute much additional flux uncertainty.

353 Our results suggest that the most important way to improve reliability of the flux estimate is  
354 to reduce the usage of gap-filled data. The current approach to gap filling in `neonSoilFlux`  
355 uses monthly mean data to gap fill—this approach decreases the ability of the estimate to be  
356 responsive to short-term pulses that occur with rapid weather shifts. Four sites (KONZ, SRER,  
357 WREF, and UNDE) had more than 75% of half-hourly periods with no-gap filled measurements  
358 (Figure S1, Supplementary Information). Two sites (SJER and WOOD) had more than 75% of  
359 half-hourly intervals with just one gap-filled measurement. The large uncertainty evident in  
360 Figure 4 for estimates from WOOD and SJER are thus due in part to the gap-filling used in  
361 these sites (Figure S1). While we did not need to use gap-filled measurements to compute the  
362 flux at WREF, field data collection occurred following a severe rainstorm, with soils at the  
363 beginning of the sampling week near their water holding capacity. In general, we recommend  
364 that whenever possible, knowledge of local field conditions should influence analysis decisions  
365 in addition to any QA filtering protocols in the `neonSoilFlux` package.

366 We recognize that this gap-filling approach may lead to gap-filled values that are quite different  
367 from the actual values, such as an underestimate of soil moisture following rain events. Further  
368 extensions of the gap filling method could use more sophisticated gap-filling routines, similar to  
369 what is used for net ecosystem carbon exchange (Falge et al., 2001; Liu et al., 2023; Mariethoz  
370 et al., 2015; Moffat et al., 2007; Zhang et al., 2023). Additionally, since the deepest temperature  
371 and soil moisture sensors are located below the deepest CO<sub>2</sub> sensors at NEON sites, it is  
372 possible that excluding these deeper layers from consideration prior to analysis would lead to a

373 reduced need for gap filling. Future iterations of the `neonSoilFlux` package may incorporate  
374 this as an option. The current gap-filling routine provides a consistent approach that can be  
375 applied to each data stream, but further work may explore alternative gap-filling approaches.

376 **6.2 Evaluation of flux-gradient approach at each site**

377 Derived results from the `neonSoilFlux` package have patterns that are broadly consistent with  
378 those directly measured in the field (Figure 4 and Figure 5), even though statistical comparisons  
379 between the field-measured and `neonSoilFlux` values were quite variable (e.g.  $R^2$  ranging  
380 from 0.04 to 0.81; Figure 6). One advantage of the `neonSoilFlux` package is its ability to  
381 calculate fluxes across different soil depths (Figure 3), which allows for additional site-specific  
382 customization. We believe the package can provide a useful baseline estimate of soil fluxes that  
383 can always be complemented through additional field measurements.

384 The six locations studied provide a range of case studies that suggest different considerations  
385 may apply to different sites when applying the flux-gradient method. For example, the Santa  
386 Rita Experimental Range (SRER) is a desert site characterized by sandy soil, which also was  
387 the location of the highest field soil temperatures that we observed (Table 2). At SRER the  
388 flux across the top two layers ( $F_{110}$ ) produced a pattern of soil flux most consistent with the  
389 observed field data. The remaining methods  $F_{101}$ ,  $F_{011}$ , or  $F_{000}$  are derived from information  
390 taken from the deepest layer, which seems to have been decoupled from the surface layers both  
391 in terms of temperature and CO<sub>2</sub> concentration. This may be a general circumstance where  
392 there are large diurnal temperature extremes that rapidly change during the course of a day  
393 and overnight, leading to lags in the timing of when temperature increases propagate down to  
394 deeper soil layers.

395 Immediately prior to our visit to Konza Prairie (KONZ), that site that experienced a significant

396 rain event that led to wet soils that gradually dried out over the course of our time there.  
397 This pulse of precipitation increased the soil CO<sub>2</sub> concentration at the top layer above the  
398 concentrations in lower layers, leading to negative estimated flux values at the start of the field  
399 sampling period. In this case it was only when the soil began to return to a baseline level that  
400 the assumptions of the flux-gradient method were again met.

401 Both of the previous cases also provide context for the variable statistical comparisons between  
402 field-measured soil fluxes and `neonSoilFlux` outputs (Figure 6). When considering systematic  
403 deployment of this method across a measurement network, there are a number of independent  
404 challenges that require careful consideration. There are clear tradeoffs between (1) accuracy of  
405 modeled fluxes (defined here as closeness to field-measured  $F_S$  and the uncertainty reduction  
406 factor  $\epsilon$ ), (2) precision (which could be defined by the signal to noise ratio), and (3) the  
407 choice of the diffusivity model (Section 4.2.2) or flux computation method (Section 4.2.3). A  
408 sensitivity analysis (Figure S2, Supplemental Information) found that flux output uncertainty  
409 was dominated by measurement uncertainty ( $T_S$ ,  $P$ ,  $SWC$ , or CO<sub>2</sub>) rather than by the diffusivity  
410 method used to compute soil flux. Notably, the  $F_{110}$  method was least sensitive to measurement  
411 uncertainty likely because it best aligns with the surface chamber measurement assumptions.

412 Finally, comparing the effects of different diffusivity estimation methods on the match between  
413 modeled and measured fluxes (Figure 5) highlights the sensitivity of  $F_{ijk}$  to diffusivity. The  
414 comparison between diffusivity estimates compared to field estimated diffusivity (Figure 7)  
415 demonstrates that site parameters can dictate which measure of diffusivity is most likely to be  
416 accurate in a given environmental context. Site-specific differences are largely a reflection of  
417 differences in soil moisture across the sites (Table 1), as not all diffusivity estimation methods  
418 incorporate soil moisture equivalently. While we here have compares two approaches to calculate  
419 diffusivity (the Millington-Quirk and Marshall models), it may be valuable to evaluate other  
420 diffusivity models (e.g. the Moldrup model; Moldrup et al. (1999)) as well. Ultimately the

<sup>421</sup> choice of a particular diffusivity model could be determined based on knowledge of site-specific  
<sup>422</sup> evaluations or a set of these models could be used to generate a model ensemble average as a  
<sup>423</sup> means to trade precision for a more general approach.

<sup>424</sup> **6.3 Recommendations for future method development**

<sup>425</sup> The `neonSoilFlux` package provides several approaches to estimate soil flux using the gradient  
<sup>426</sup> method. We believe these approaches enable the software to be used across a range of site-  
<sup>427</sup> specific assumptions (Maier & Schack-Kirchner, 2014). We note, however, that this choice  
<sup>428</sup> can have a determinative approach on the calculated values. Ensemble averaging approaches  
<sup>429</sup> (Elshall et al., 2018; Raftery et al., 2005) may be one way to address this problem if the goal is  
<sup>430</sup> to calculate fluxes using the same method at a diverse range of different sites. Two other ideas  
<sup>431</sup> would be to apply machine learning algorithms (e.g. random forest) to generate a single flux  
<sup>432</sup> estimate across diverse sites, or using co-located estimates of net ecosystem carbon exchange  
<sup>433</sup> from eddy-flux towers to further constrain results or to assess soil flux results for plausibility  
<sup>434</sup> (Phillips et al., 2017).

<sup>435</sup> These challenges notwithstanding, the method used here and made available in the  
<sup>436</sup> `neonSoilFlux` R package has the potential to produce nearly continuous estimates of flux  
<sup>437</sup> across all terrestrial NEON sites. These estimates are a significant improvement on available  
<sup>438</sup> approaches to constrain the portion of ecosystem respiration attributable to the soil. This, in  
<sup>439</sup> turn, also aids in our ability to understand the soil contribution to the net ecosystem flux  
<sup>440</sup> measured at these sites using the co-located eddy flux towers.

<sup>441</sup> **7 Conclusions**

<sup>442</sup> We used the R package `neonSoilFlux` to estimate soil CO<sub>2</sub> fluxes with the flux-gradient method  
<sup>443</sup> using data from buried soil sensors at NEON terrestrial sites. We compared the predicted  
<sup>444</sup> fluxes to those measured directly using a field-based closed chamber approach. Soil fluxes  
<sup>445</sup> from `neonSoilFlux` were broadly effective at producing estimates of flux comparable to those  
<sup>446</sup> measured in the field using a chamber-based technique. However `neonSoilFlux` outputs are  
<sup>447</sup> quite sensitive to a number of issues, including: missing data (and thus gap-filling of input  
<sup>448</sup> measurement datasets), the selection of soil depths used to best calculate the gradient (which  
<sup>449</sup> may vary between sites), and finally the choice of method used for estimating soil diffusivity.  
<sup>450</sup> The flexibility of the `neonSoilFlux` package allows the user to evaluate each of these issues  
<sup>451</sup> with site-specific knowledge and contexts. Future refinements and subsequent validation of  
<sup>452</sup> `neonSoilFlux` outputs will feed forward into evaluating soil carbon fluxes broader spatial scales  
<sup>453</sup> to enhance understanding of the ways in which soils across diverse ecosystems are responding  
<sup>454</sup> to a changing climate.

<sup>455</sup> **Sources Cited**

- <sup>456</sup> Ayres, E., Reichle, R. H., Colliander, A., Cosh, M. H., & Smith, L. (2024). Validation of  
<sup>457</sup> Remotely Sensed and Modeled Soil Moisture at Forested and Unforested NEON Sites.  
<sup>458</sup> *IEEE Journal of Selected Topics in Applied Earth Observations and Remote Sensing*, 17,  
<sup>459</sup> 14248–14264. <https://doi.org/10.1109/JSTARS.2024.3430928>
- <sup>460</sup> Baldocchi, D. (2014). Measuring fluxes of trace gases and energy between ecosystems and the  
<sup>461</sup> atmosphere - the state and future of the eddy covariance method. *Global Change Biology*,  
<sup>462</sup> 20(12), 3600–3609. <https://doi.org/10.1111/gcb.12649>

- 463 Berenbaum, M. R., Carpenter, S. R., Hampton, S. E., Running, S. W., & Stanzione, D. C.  
464 (2015). *Report from the NSF BIO Advisory Committee Subcommittee on NEON Scope*  
465 *Impacts*.
- 466 Bond-Lamberty, B. (2018). New Techniques and Data for Understanding the Global Soil  
467 Respiration Flux. *Earth's Future*, 6(9), 1176–1180. <https://doi.org/10.1029/2018EF000866>
- 468 Bond-Lamberty, B., Ballantyne, A., Berryman, E., Fluet-Chouinard, E., Jian, J., Morris, K.  
469 A., Rey, A., & Vargas, R. (2024). Twenty Years of Progress, Challenges, and Opportunities  
470 in Measuring and Understanding Soil Respiration. *Journal of Geophysical Research: Biogeosciences*, 129(2), e2023JG007637. <https://doi.org/10.1029/2023JG007637>
- 472 Bond-Lamberty, B., Christianson, D. S., Malhotra, A., Pennington, S. C., Sihi, D., AghaK-  
473 ouchak, A., Anjileli, H., Altaf Arain, M., Armesto, J. J., Ashraf, S., Ataka, M., Baldocchi,  
474 D., Andrew Black, T., Buchmann, N., Carbone, M. S., Chang, S.-C., Crill, P., Curtis, P.  
475 S., Davidson, E. A., ... Zou, J. (2020). COSORE: A community database for continuous  
476 soil respiration and other soil-atmosphere greenhouse gas flux data. *Global Change Biology*,  
477 26(12), 7268–7283. <https://doi.org/10.1111/gcb.15353>
- 478 Bond-Lamberty, B., & Thomson, A. (2010). A global database of soil respiration data.  
479 *Biogeosciences*, 7(6), 1915–1926. <https://doi.org/10.5194/bg-7-1915-2010>
- 480 Bond-Lamberty, B., Wang, C., & Gower, S. T. (2004). A global relationship between the  
481 heterotrophic and autotrophic components of soil respiration? *Global Change Biology*,  
482 10(10), 1756–1766. <https://doi.org/10.1111/j.1365-2486.2004.00816.x>
- 483 Bouma, T. J., & Bryla, D. R. (2000). On the assessment of root and soil respiration for soils of  
484 different textures: Interactions with soil moisture contents and soil CO<sub>2</sub> concentrations.  
485 *Plant and Soil*, 227(1), 215–221. <https://doi.org/10.1023/A:1026502414977>
- 486 Chen, H., & Tian, H.-Q. (2005). Does a General Temperature-Dependent Q10 Model of Soil  
487 Respiration Exist at Biome and Global Scale? *Journal of Integrative Plant Biology*, 47(11),  
488 1288–1302. <https://doi.org/10.1111/j.1744-7909.2005.00211.x>

- 489 Davidson, E. A., Janssens, I. A., & Luo, Y. (2006). On the variability of respiration in  
490 terrestrial ecosystems: Moving beyond Q10. *Global Change Biology*, 12, 154–164. <https://doi.org/10.1111/j.1365-2486.2005.01065.x>
- 491
- 492 Desai, A. R., Murphy, B. A., Wiesner, S., Thom, J., Butterworth, B. J., Koupaei-Abyazani, N.,  
493 Muttaqin, A., Paleri, S., Talib, A., Turner, J., Mineau, J., Merrelli, A., Stoy, P., & Davis,  
494 K. (2022). Drivers of Decadal Carbon Fluxes Across Temperate Ecosystems. *Journal of*  
495 *Geophysical Research: Biogeosciences*, 127(12), e2022JG007014. <https://doi.org/10.1029/2022JG007014>
- 496
- 497 Efron, B., & Tibshirani, R. J. (1994). *An Introduction to the Bootstrap*. Chapman and  
498 Hall/CRC. <https://doi.org/10.1201/9780429246593>
- 499 Elshall, A. S., Ye, M., Pei, Y., Zhang, F., Niu, G.-Y., & Barron-Gafford, G. A. (2018). Relative  
500 model score: A scoring rule for evaluating ensemble simulations with application to microbial  
501 soil respiration modeling. *Stochastic Environmental Research and Risk Assessment*, 32(10),  
502 2809–2819. <https://doi.org/10.1007/s00477-018-1592-3>
- 503 Falge, E., Baldocchi, D., Olson, R., Anthoni, P., Aubinet, M., Bernhofer, C., Burba, G.,  
504 Ceulemans, R., Clement, R., Dolman, H., Granier, A., Gross, P., Grünwald, T., Hollinger,  
505 D., Jensen, N.-O., Katul, G., Keronen, P., Kowalski, A., Lai, C. T., ... Wofsy, S. (2001).  
506 Gap filling strategies for defensible annual sums of net ecosystem exchange. *Agricultural*  
507 *and Forest Meteorology*, 107(1), 43–69. [https://doi.org/10.1016/S0168-1923\(00\)00225-2](https://doi.org/10.1016/S0168-1923(00)00225-2)
- 508 Farrance, I., & Frenkel, R. (2012). Uncertainty of Measurement: A Review of the Rules  
509 for Calculating Uncertainty Components through Functional Relationships. *The Clinical*  
510 *Biochemist Reviews*, 33(2), 49–75.
- 511 Friedlingstein, P., O’Sullivan, M., Jones, M. W., Andrew, R. M., Hauck, J., Landschützer,  
512 P., Le Quéré, C., Li, H., Luijkx, I. T., Olsen, A., Peters, G. P., Peters, W., Pongratz,  
513 J., Schwingshackl, C., Sitch, S., Canadell, J. G., Ciais, P., Jackson, R. B., Alin, S. R., ...  
514 Zeng, J. (2025). Global Carbon Budget 2024. *Earth System Science Data*, 17(3), 965–1039.

- 515        <https://doi.org/10.5194/essd-17-965-2025>
- 516    Hamdi, S., Moyano, F., Sall, S., Bernoux, M., & Chevallier, T. (2013). Synthesis analysis  
517        of the temperature sensitivity of soil respiration from laboratory studies in relation to  
518        incubation methods and soil conditions. *Soil Biology and Biochemistry*, 58, 115–126.
- 519        <https://doi.org/10.1016/j.soilbio.2012.11.012>
- 520    Jackson, R. B., Lajtha, K., Crow, S. E., Hugelius, G., Kramer, M. G., & Piñeiro, G. (2017).  
521        The Ecology of Soil Carbon: Pools, Vulnerabilities, and Biotic and Abiotic Controls.  
522        *Annual Review of Ecology, Evolution and Systematics*, 48(Volume 48, 2017), 419–445.  
523        <https://doi.org/10.1146/annurev-ecolsys-112414-054234>
- 524    Jian, J., Bailey, V., Dorheim, K., Konings, A. G., Hao, D., Shiklomanov, A. N., Snyder,  
525        A., Steele, M., Teramoto, M., Vargas, R., & Bond-Lamberty, B. (2022). Historically  
526        inconsistent productivity and respiration fluxes in the global terrestrial carbon cycle. *Nature  
527        Communications*, 13(1), 1733. <https://doi.org/10.1038/s41467-022-29391-5>
- 528    Jian, J., Vargas, R., Anderson-Teixeira, K., Stell, E., Herrmann, V., Horn, M., Kholod, N.,  
529        Manzon, J., Marchesi, R., Paredes, D., & Bond-Lamberty, B. (2021). A restructured and  
530        updated global soil respiration database (SRDB-V5). *Earth System Science Data*, 13(2),  
531        255–267. <https://doi.org/10.5194/essd-13-255-2021>
- 532    Jiang, J., Feng, L., Hu, J., Liu, H., Zhu, C., Chen, B., & Chen, T. (2024). Global soil  
533        respiration predictions with associated uncertainties from different spatio-temporal data  
534        subsets. *Ecological Informatics*, 82, 102777. <https://doi.org/10.1016/j.ecoinf.2024.102777>
- 535    Jobbágy, E. G., & Jackson, R. B. (2000). The Vertical Distribution of Soil Organic Carbon  
536        and its Relation to Climate and Vegetation. *Ecological Applications*, 10(2), 423–436.  
537        [https://doi.org/10.1890/1051-0761\(2000\)010%5B0423:TVDOSO%5D2.0.CO;2](https://doi.org/10.1890/1051-0761(2000)010%5B0423:TVDOSO%5D2.0.CO;2)
- 538    Jurasinski, G., Koebisch, F., Guenther, A., & Beetz, S. (2022). *Flux: Flux Rate Calculation  
539        from Dynamic Closed Chamber Measurements*.
- 540    Liu, K., Li, X., Wang, S., & Zhang, H. (2023). A robust gap-filling approach for European

- 541 Space Agency Climate Change Initiative (ESA CCI) soil moisture integrating satellite  
542 observations, model-driven knowledge, and spatiotemporal machine learning. *Hydrology*  
543 and *Earth System Sciences*, 27(2), 577–598. <https://doi.org/10.5194/hess-27-577-2023>
- 544 Lunch, C., Laney, C., Mietkiewicz, N., Sokol, E., Cawley, K., & Network), N. (National. E. O.  
545 (2025). *neonUtilities: Utilities for Working with NEON Data*.
- 546 Luo, Y., Ogle, K., Tucker, C., Fei, S., Gao, C., LaDeau, S., Clark, J. S., & Schimel, D. S. (2011).  
547 Ecological forecasting and data assimilation in a data-rich era. *Ecological Applications*,  
548 21(5), 1429–1442. <https://doi.org/10.1890/09-1275.1>
- 549 Maier, M., & Schack-Kirchner, H. (2014). Using the gradient method to determine soil gas  
550 flux: A review. *Agricultural and Forest Meteorology*, 192–193, 78–95. <https://doi.org/10.1016/j.agrformet.2014.03.006>
- 552 Mariethoz, G., Linde, N., Jougnot, D., & Rezaee, H. (2015). Feature-preserving interpolation  
553 and filtering of environmental time series. *Environmental Modelling & Software*, 72, 71–76.  
554 <https://doi.org/10.1016/j.envsoft.2015.07.001>
- 555 Marshall, T. J. (1959). The Diffusion of Gases Through Porous Media. *Journal of Soil Science*,  
556 10(1), 79–82. <https://doi.org/10.1111/j.1365-2389.1959.tb00667.x>
- 557 Millington, R. J., & Shearer, R. C. (1971). Diffusion in aggregated porous media. *Soil Science*,  
558 111(6), 372–378.
- 559 Moffat, A. M., Papale, D., Reichstein, M., Hollinger, D. Y., Richardson, A. D., Barr, A. G.,  
560 Beckstein, C., Braswell, B. H., Churkina, G., Desai, A. R., Falge, E., Gove, J. H., Heimann,  
561 M., Hui, D., Jarvis, A. J., Kattge, J., Noormets, A., & Stauch, V. J. (2007). Comprehensive  
562 comparison of gap-filling techniques for eddy covariance net carbon fluxes. *Agricultural and*  
563 *Forest Meteorology*, 147(3), 209–232. <https://doi.org/10.1016/j.agrformet.2007.08.011>
- 564 Moldrup, P., Olesen, T., Yamaguchi, T., Schjønning, P., & Rolston, D. E. (1999). Modeling  
565 diffusion and reaction in soils: 9. The Buckingham-Burdine-Campbell equation for gas  
566 diffusivity in undisturbed soil. *Soil Science*, 164(2), 75.

- 567 NEON. (2024a). *Barometric pressure (DP1.00004.001)*. National Ecological Observatory  
568 Network (NEON). <https://doi.org/10.48443/RT4V-KZ04>
- 569 NEON. (2024b). *Soil CO<sub>2</sub> concentration (DP1.00095.001)*. National Ecological Observatory  
570 Network (NEON). <https://doi.org/10.48443/E7GR-6G94>
- 571 NEON. (2024c). *Soil physical and chemical properties, Megapit (DP1.00096.001)*. National  
572 Ecological Observatory Network (NEON). <https://doi.org/10.48443/S6ND-Q840>
- 573 NEON. (2024d). *Soil temperature (DP1.00041.001)*. National Ecological Observatory Network  
574 (NEON). <https://doi.org/10.48443/Q24X-PW21>
- 575 NEON. (2024e). *Soil water content and water salinity (DP1.00094.001)*. National Ecological  
576 Observatory Network (NEON). <https://doi.org/10.48443/A8VY-Y813>
- 577 Norman, J. M., Kucharik, C. J., Gower, S. T., Baldocchi, D. D., Crill, P. M., Rayment,  
578 M., Savage, K., & Striegl, R. G. (1997). A comparison of six methods for measuring  
579 soil-surface carbon dioxide fluxes. *Journal of Geophysical Research: Atmospheres*, 102(D24),  
580 28771–28777. <https://doi.org/10.1029/97JD01440>
- 581 Pedersen, A. R. (2024). *HMR: Flux Estimation with Static Chamber Data*.
- 582 Phillips, C. L., Bond-Lamberty, B., Desai, A. R., Lavoie, M., Risk, D., Tang, J., Todd-Brown,  
583 K., & Vargas, R. (2017). The value of soil respiration measurements for interpreting and  
584 modeling terrestrial carbon cycling. *Plant and Soil*, 413(1), 1–25. <https://doi.org/10.1007/s11104-016-3084-x>
- 586 Raftery, A. E., Gneiting, T., Balabdaoui, F., & Polakowski, M. (2005). *Using Bayesian Model  
587 Averaging to Calibrate Forecast Ensembles*. <https://doi.org/10.1175/MWR2906.1>
- 588 Rheault, K., Christiansen, J. R., & Larsen, K. S. (2024). goFlux: A user-friendly way to  
589 calculate GHG fluxes yourself, regardless of user experience. *Journal of Open Source  
590 Software*, 9(96), 6393. <https://doi.org/10.21105/joss.06393>
- 591 Sallam, A., Jury, W. A., & Letey, J. (1984). Measurement of Gas Diffusion Coefficient under  
592 Relatively Low Air-filled Porosity. *Soil Science Society of America Journal*, 48(1), 3–6.

- 593        <https://doi.org/10.2136/sssaj1984.03615995004800010001x>
- 594    Shao, J., Zhou, X., Luo, Y., Li, B., Aurela, M., Billesbach, D., Blanken, P. D., Bracho, R.,  
595        Chen, J., Fischer, M., Fu, Y., Gu, L., Han, S., He, Y., Kolb, T., Li, Y., Nagy, Z., Niu, S.,  
596        Oechel, W. C., ... Zhang, J. (2015). Biotic and climatic controls on interannual variability  
597        in carbon fluxes across terrestrial ecosystems. *Agricultural and Forest Meteorology*, 205,  
598        11–22. <https://doi.org/10.1016/j.agrformet.2015.02.007>
- 599    Shao, P., Zeng, X., Moore, D. J. P., & Zeng, X. (2013). Soil microbial respiration from  
600        observations and Earth System Models. *Environmental Research Letters*, 8(3), 034034.  
601        <https://doi.org/10.1088/1748-9326/8/3/034034>
- 602    Sihi, D., Gerber, S., Inglett, P. W., & Inglett, K. S. (2016). Comparing models of microbial–  
603        substrate interactions and their response to warming. *Biogeosciences*, 13(6), 1733–1752.  
604        <https://doi.org/10.5194/bg-13-1733-2016>
- 605    Tang, J., Baldocchi, D. D., Qi, Y., & Xu, L. (2003). Assessing soil CO<sub>2</sub> efflux using continuous  
606        measurements of CO<sub>2</sub> profiles in soils with small solid-state sensors. *Agricultural and Forest  
607        Meteorology*, 118(3), 207–220. [https://doi.org/10.1016/S0168-1923\(03\)00112-6](https://doi.org/10.1016/S0168-1923(03)00112-6)
- 608    Tang, J., Misson, L., Gershenson, A., Cheng, W., & Goldstein, A. H. (2005). Continuous  
609        measurements of soil respiration with and without roots in a ponderosa pine plantation  
610        in the Sierra Nevada Mountains. *Agricultural and Forest Meteorology*, 132(3), 212–227.  
611        <https://doi.org/10.1016/j.agrformet.2005.07.011>
- 612    Taylor, J. R. (2022). *An Introduction to Error Analysis: The Study of Uncertainties in Physical  
613        Measurements, Third Edition* (3rd ed.). University Science Press.
- 614    Wilson, S. J., Bond-Lamberty, B., Noyce, G., Bittencourt Peixoto, R., & Megonigal, J. P.  
615        (2024). Fluxfinder: An R Package for Reproducible Calculation and Initial Processing  
616        of Greenhouse Gas Fluxes From Static Chamber Measurements. *Journal of Geophysical  
617        Research: Biogeosciences*, 129(11), e2024JG008208. <https://doi.org/10.1029/2024JG008208>
- 618    Yan, Z., Bond-Lamberty, B., Todd-Brown, K. E., Bailey, V. L., Li, S., Liu, C., & Liu, C. (2018).

- 619 A moisture function of soil heterotrophic respiration that incorporates microscale processes.
- 620 *Nature Communications*, 9(1), 2562. <https://doi.org/10.1038/s41467-018-04971-6>
- 621 Yan, Z., Liu, C., Todd-Brown, K. E., Liu, Y., Bond-Lamberty, B., & Bailey, V. L. (2016).
- 622 Pore-scale investigation on the response of heterotrophic respiration to moisture conditions
- 623 in heterogeneous soils. *Biogeochemistry*, 131(1), 121–134. <https://doi.org/10.1007/s10533-016-0270-0>
- 625 Zhang, R., Kim, S., Kim, H., Fang, B., Sharma, A., & Lakshmi, V. (2023). Temporal Gap-Filling
- 626 of 12-Hourly SMAP Soil Moisture Over the CONUS Using Water Balance Budgeting. *Water*
- 627 *Resources Research*, 59(12), e2023WR034457. <https://doi.org/10.1029/2023WR034457>
- 628 Zhao, J. (2019). FluxCalR: A R package for calculating CO<sub>2</sub> and CH<sub>4</sub> fluxes from static
- 629 chambers. *Journal of Open Source Software*, 4(43), 1751. <https://doi.org/10.21105/joss.01751>
- 631 Zobitz, J., Ayres, E., O'Rourke, K., Werbin, Z., Lee, L., Abdi, R., Mehmeti, D., & Xiong, L.
- 632 (2024). *neonSoilFlux: Compute Soil Carbon Fluxes for the National Ecological Observatory*
- 633 *Network Sites*.
- 634 Zobitz, J., & Zimmerman, N. (2025). *Supporting Code and Data for neonSoilFlux: An R*
- 635 *Package for Continuous Sensor-Based Estimation of Soil CO<sub>2</sub> Fluxes*. Zenodo. <https://doi.org/10.5281/zenodo.17516320>